X-ray-diffraction studies of Co/Re superlattices

Y. Huai* and R. W. Cochrane*
Département de Physique et Groupe de Recherche en Physique et Technologie des Couches Minces, Université de Montréal, Case Postale 6128, Succursale A, Montréal, Québec, Canada H3C 3J7

M. Sutton
Department of Physics, Centre for the Physics of Materials, McGill University, 3600 University Street, Montréal, Québec, Canada H3A 2T8

(Received 14 August 1992; revised manuscript received 16 March 1993)

The structural properties of sputtered Co/Re equal-thickness superlattices and several Co/Re bilayer films have been investigated using x-ray diffraction. Low-angle x-ray-reflectvity data have been analyzed using an optical model which includes both interfacial mixing and discrete layer-thickness fluctuations. The fits to the bilayer reflectivity data indicate that interfacial mixing is limited to $\sim 2-3$ monolayers for Re deposited on Co, and that a very sharp interface is found for Co deposited on Re. Such an asymmetric interfacial configuration has been confirmed by the fitted results from the superlattice reflectivity data. Somewhat larger average intermixing widths ($\sim 3-5$ monolayers) are found in the superlattices and are attributed to the cumulatively increased layer roughness with increasing layer distance from the substrate. High-angle x-ray-diffraction data show that superlattice films have coherent interfaces and a highly textured structure with hcp [002] orientations normal to the plane for periods $41 \leq \Lambda \leq 220$ Å. Detailed structures have been determined by fitting the x-ray-diffraction spectra to calculated spectra using a trapezoidal model which considers crystalline multilayer films having extended interfaces with linear composition profiles. The fitted results of the high-angle diffraction spectra are in good agreement with the results obtained from the reflectivity data. In addition, an out-of-plane expansion of the Co(002) layer is observed in all samples and is interpreted to be a consequence of structural disorder which leads to a slightly reduced atomic density.

I. INTRODUCTION

An increasing interest in artificially layered materials consisting of magnetic and nonmagnetic layers arises from the recent discovery of giant magnetoresistance[1] and perpendicular magnetic anisotropy,[2] both of which demonstrate their potential for applications.[1,2] Such physical properties depend strongly on the atomic structure of the individual layers, the interfacial configurations, and the coherence between layers. A complete structural examination is then a very important step for understanding the transport and magnetic properties of these multilayer materials. X-ray diffraction is a widely used technique to characterize the structure of multilayers,[3] since it is both nondestructive and straightforward to perform. Moreover, detailed structural information can be obtained by modeling the multilayer structures and comparing the calculated x-ray intensity of the modeled structures with experimental data.[4,5]

In this paper, we report the structural properties of Co/Re superlattice films $[\mathrm{Co}(t_a)/\mathrm{Re}(t_b)]_N$ with equal-layer thicknesses ($t_a = t_b = 7-110$ Å) and several bilayer films investigated by low- and high-angle x-ray diffraction. Our interest in the Co/Re system was motivated by recently observed oscillatory magnetic interlayer coupling and spin-valve magnetoresistance in magnetic multilayers.[1,6] Co and Re each crystallize in a hcp crystal structure (type Mg) with α-Co having $a = 2.507$ Å, $c = 4.069$ Å and Re having $a = 2.761$ Å, $c = 4.458$ Å. As a result, there is a lattice mismatch of 9.2% between the two lattices for multilayers oriented in the [002] direction. On the other hand, the Co/Re system has a small positive heat of mixing[7] of 1 kJ/g-at. and the alloy-phase diagram shows a continuous solid solubility of the two elements,[8] so that crystalline alloy interfaces are expected in multilayer films. Since complexities arise in the multilayer structures from layer-thickness fluctuations, several bilayer films have also been prepared under the same conditions as the multilayer films in order to facilitate the examination of interfacial mixing.

The remainder of this paper is organized as follows. In Sec. II, the sputtering system and the sample preparation process are briefly described along with the details of x-ray measurements and the fitting procedure. In Sec. III, an optical model is outlined that includes both a linear intermixing profile and discrete layer-thickness fluctuations, and the fitted results from the bilayer and multilayer reflectivities are presented. In Sec. IV, the trapezoidal model is described and applied to the analysis of the high-angle diffraction data, and in Sec. V the high-angle fitted results are compared with the low-angle reflectivity parameters. The magnetic properties of these Co/Re equal-thickness structures will be presented elsewhere.[9]

II. EXPERIMENTAL DETAILS

A. Sample preparation and characterization

Single and multiple Co/Re bilayer films were prepared using a modified single-source rf triode sputtering system.[10] In this system, two separated targets (99.9% Co and 99.99% Re) were clamped to a water-cooled target support (cathode) powered by a single rf power supply. Beam confinement and isolation shields were set over the targets to avoid intermixing the fluxes of the sputtered atoms. Electron microprobe analysis of pure Co and Re samples prepared over each target indicates that the two atomic fluxes were well separated. Deposition rates of the two elements Co and Re were individually measured with a quartz-crystal monitor in place of the substrate, and were precisely calibrated using x-ray-reflectivity measurements. In subsequent experiments, individual layer thicknesses in bilayer and multilayer samples were regulated by computer control of the substrate position and the exposure time. Prior to sputtering, the base pressure was $\leq 1\times10^{-7}$ Torr. During sputtering, the substrate temperature rose to about 40 °C. With a sputtering pressure of 7.5 mTorr of argon gas (99.999%), the typical deposition rates were 1.9 Å/s for Co and 2.5 Å/s for Re at a rf power of 88 W and a substrate-target distance of 5.5 cm. Films were deposited onto degreased glass substrates (Corning 7059 1×2 cm^2) or oxidized Si(100) wafers through masks which defined the sample dimensions appropriate for x-ray and transport measurements.

Total film thickness and average film composition were checked with a DEKTAK step profiler and an electron microprobe, respectively. Due to the atomic size difference of Co and Re, the equal-layer-thickness samples have an average composition $Co_{57.3}Re_{42.7}$; the measured composition from electron microprobe for all samples is consistent to within 4% with this calculated one. In addition, an x-ray photoemission spectroscopy (XPS) evaluation of a number of samples was undertaken to check for oxidation of the constituents during sputtering. No peaks related to Co and Re oxide states were detected on the sample surfaces cleaned by Ar^+ sputtering in a high vacuum chamber.

B. X-ray measurements

X-ray-reflectivity experiments were performed using a high-resolution triple-axis diffractometer with a Cu-$K\alpha$ sealed tube. By using a single-crystal Ge(111) monochromater and analyzer, a resolution of order 0.01°, full width at half maximum (FWHM), for a θ-2θ scan was achieved, corresponding to a ΔQ of 0.0004 Å^{-1} (FWHM) in reciprocal space. The initial alignment procedure for each sample was to block half the $K\alpha_1$ x-ray beam at $\theta=0$. Since the low-angle reflectivity data are very sensitive to the alignment of the samples and the diffractometer, extreme care was taken in order to maintain the same alignment conditions for all samples. After complete aligning of the sample, a θ-2θ scan (longitudinal) was taken to measure the specular reflection signal and rocking curve (commonly called the transverse or ω scan) was also measured by rocking the sample through the specular reflection with fixed 2θ. High-angle x-ray-diffraction measurements, including θ-2θ symmetric reflection and transmission scans (with a scattering vector perpendicular to or lying in the film plane) and rocking curves were carried out on a conventional powder diffractometer with Cu-$K\alpha$ radiation. The instrumental broadening for this diffractometer was estimated from Al powder diffraction measurements to be 0.15°, FWHM, for a θ-2θ scan.

C. Fitting procedure

In order to extract the appropriate physical parameters from the low-angle reflectivity and the high-angle diffraction data, model calculations (described in the following sections) are fit to the data using a nonlinear least-squares procedure which minimizes

$$\chi^2=\sum_{i=1}^{M}(R_i^m-R_i^c)^2/\sigma_i^2 , \tag{1}$$

where R_i^m and R_i^c are the experimental and calculated x-ray intensities, respectively, M is the total number of data points, and σ_i^2 is the weighting function. Considering that the x-ray intensities vary over more than four orders of magnitude, the choice of σ_i^2 is very important. At high reflected intensities, errors of a few percent, arising from variation in the beam intensity and sample alignment, can be significantly larger than those calculated on the basis of counting statistics. Within the low-angle model calculations, the approximate form of the "footprint" corrections[11] applied to the calculated intensity contributes an additional nonrandom uncertainty which is also better treated as a percentage error rather than a counting statistic. At low reflected intensities, a σ_i^2 determined by the counting statistics and proportional to the number of counts is the appropriate form. Recognizing these facts, several authors[4,5] have proposed an intermediate form $\sigma_i^2=(R_i^m)^\varepsilon$, with $1\leq\varepsilon\leq2$, although there appears to be no compelling rationale for a particular choice of ε. In our approach, the overall weighting factor is calculated as the sum of two terms arising from a percentage uncertainty at high intensities and counting statistics at low intensities, giving

$$\sigma_i^2=R_i^m+(\alpha R_i^m)^2 , \tag{2}$$

α being the fractional uncertainty. This form interpolates smoothly, but in a nonlinear fashion as a function of α, between the two terms. In a series of fitting tests to bilayer reflectivity data, stationary values of the layer and interface parameters were found for α values in the range from 1% to 10%, consistent with our estimate of the systematic error. Moreover, α values in this range reproduce almost exactly the solutions obtained with the intermediate forms, $\sigma_i^2=(R_i^m)^\varepsilon$. The fits reported in this paper typically use $\alpha\sim0.05$.

III. X-RAY-REFLECTIVITY ANALYSIS

A. Reflectivity calculation

The x-ray-reflectivity data analysis is based on a standard optical model.[12] The refractive index n of most ma-

terials in the x-ray wavelength range is slightly less than 1, and can be written as $n=1-\delta-i\beta$, where δ and β can be expressed as

$$\delta=\frac{\mathcal{N}_0 r_e\lambda^2}{2\pi}(f_0+\Delta f')=\frac{r_e\lambda^2}{2\pi}\rho_e\ , \tag{3}$$

$$\beta=\frac{\mathcal{N}_0 r_e\lambda^2}{2\pi}(\Delta f'')=\frac{\lambda}{4\pi}\mu\ , \tag{4}$$

where r_e is the classical electron radius $e^2/mc^2=2.818\times10^{-13}$ cm, $\mathcal{N}_0$ is the number density of atoms, λ is the x-ray wavelength, f_0 is the atomic scattering factor at zero momentum transfer and is equal to Z, the atomic number of the considered element, $\Delta f'$ and $\Delta f''$ are the real and imaginary parts of the dispersion corrections to f_0, ρ_e is the electron density, and μ is the linear absorption coefficient. The critical angle for total external reflection $\theta_c\approx\sqrt{2\delta}$ has values typically in the range 0.2°–0.6° for an x-ray wavelength around 1.5 Å. For incidence angles greater than the critical angle, most of the x-ray beam is refracted into the material, allowing interference between reflections from various interfaces, including the upper surface. If the multilayer structure is highly periodic along the film growth direction, constructive interference can be greatly enhanced to produce superlattice Bragg peaks with positions determined by the modified Bragg's law[13]

$$\sin^2\theta=\sin^2\theta_B+2\delta\ , \tag{5}$$

or simply ($\sin x\approx x$ for very small x)

$$\theta^2=\theta_B^2+\theta_c^2\ , \tag{6}$$

where θ_c is the critical angle, δ is given in Eq. (3), θ is the measured position of the diffraction peak, and θ_B is the position determined from the simple Bragg's law (neglecting refraction) $\sin\theta_B=n\lambda/2\Lambda$ (Λ is the modulation wavelength).

The x-ray reflectivity is calculated using a matrix method.[12] Any single layer in a multilayer can be characterized by a matrix (2×2) as a function of the layer thickness (t), the complex refractive index (n) (in terms of the electron density and the linear absorption coefficient), and the wave vector ($k_0=2\pi/\lambda$) of the incident beam.[12] The multilayer matrix is obtained from the product of the matrices of individual layers. In order to include interfacial mixing, a linear composition profile is assumed, and this linear interface profile is treated as a sequence of slices (~1 Å) with an average index of refraction for which the appropriate matrix is calculated. It is pointed out that other profiles with straightforward expressions[14] (such as error, sinusoidal, and exponential spatial profiles) can also be used for modeling interface profiles, but should be equivalent. A global interface roughness factor has also been incorporated into the calculation by assuming a Gaussian form [with a Debye-Waller factor $e^{-\sigma_r^2Q^2}$ multiplied to the multilayer reflectivity; here, σ_r is the root-mean-square (rms) roughness] to simulate the damping effect. It should be noted that the above optical model has been shown to be equivalent to dynamical calculations.[15] For fitting the reflectivity data to those calculated from the model, "footprint" corrections[11] and a background (0.2 counts/s of dark current in our experiment) were included in the model calculations.

B. Bilayer results

To facilitate examination of atomic intermixing at interfaces, two pairs of bilayer samples were also prepared under the same conditions as the multilayer films. Figure 1 shows the normalized x-ray-reflectivity data (open dots) along with the fitted results (solid line) using the optical model for a pair of bilayer samples prepared simultaneously. In the figure, the data and fitted results are plotted on a logarithmic scale as a function of the scattering vector $Q=4\pi\sin\theta/\lambda$. The electron densities and linear absorption coefficients of bulk Co and Re were used in the calculation. The important parameters to be adjusted are the two individual layer thicknesses ($t_{\mathrm{Co}}, t_{\mathrm{Re}}$), the interface thickness (t_i), and the root-mean-square (rms) roughness (σ_r). For two bilayer samples with Re deposited on a Co layer, excellent agreement between fitted and experimental data has been obtained without adding any top overlayer. However, for samples with Co deposited on a Re layer, it was found that good fits to the data could only be obtained by addition of an overlayer (thick-

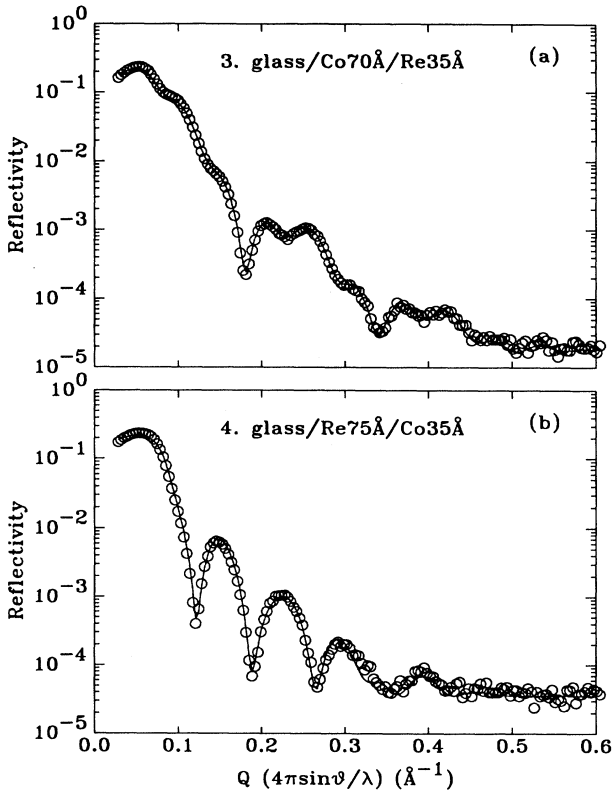

FIG. 1. X-ray-reflectivity data of a pair of bilayer samples: (a) for sample 3 and (b) for sample 4. The circles are the experimental data and the solid lines are fitted results using the optical model described in the text.

ness t_0, having nearly the CoO_2 electron density) at the Co surface. The global interface roughness σ_r values in the samples with an oxide overlayer on top of the Co are found to be slightly greater than those in samples with a Re top layer which does not oxidize. The fitted parameters for the two pairs of bilayer films are listed in Table I.

The most interesting result from the parameters listed in Table I is that the intermixing at the interfaces for the two configurations, i.e., Co deposited on Re and Re deposited on Co, are different. For samples with deposition order glass/Co/Re, the interface thickness t_i was found to be ~ 3 monolayers (ML) for sample 1 and ~ 2 ML for the thinner sample 2. For samples with deposition order glass/Re/Co, t_i is almost zero, indicating that a sharper interface is formed when Co is deposited on a Re layer, in spite of the fact that hcp Co and Re can form continuous solid solutions across the composition range. This difference could result from thermodynamic considerations arising from different surface energies for Co on Re and Re on Co, or may be due to the kinetics of the sputtering process. Whatever the origin of this effect, the structural information obtained from simple bilayer samples is a useful guide for understanding the more complex interface configurations arising on multilayer structures, which are described in Sec. III C.

C. Multilayer results

In the analysis of the bilayer reflectivity data, the global interface roughness and the interdiffusion at the interfaces between Co and Re were considered. For the multilayer structure, another type of imperfection to be considered is the variation of the bilayer thickness over a large number of periods. The different thickness disorders may arise from fluctuations and drift in the deposition rate, or from growth modes and interface disorder. It is known that interfacial mixing can reduce the higher-order main peak intensities in the reflectivity data, but it does not lead to peak broadening. In contrast, the thickness fluctuations (continuous or discrete) give rise to cumulative disorder and destroy the long-range order of the superlattice, resulting in main Bragg peak broadening (which increases with the peak order) as well as in damping of higher-order Bragg peak intensities.[16] It has been shown that the decrease of the high-order low-angle peak intensity is not necessarily due to interdiffusion at the interface, but could be caused by interface roughnesses due either to mixing or to discrete steps[17] of the lattice constant.

In order to obtain the appropriate interfacial mixing width and disorder parameters in the multilayer structures, layer-thickness disorders were included in the optical model. High-angle diffraction data (presented in Sec. IV) indicate a high degree of crystallographic order at the Co/Re interfaces, so that only discrete fluctuations in the layer thicknesses in multiples of the lattice constant are included in the model calculation. Such discrete fluctuations are modeled by selecting the layer thickness from a discrete Gaussian distribution with width Δt (typically $\Delta t \sim 1-4$ Å). The final intensity was averaged over the intensities of a larger number of such randomly selected structures (~ 100).[4,17] This procedure has an important smoothing effect on the calculated reflectivity curve (mostly for higher-order peaks) and, in effect, simulates many local domains within the area illuminated by the x-ray beam, each of which contains a different sequence of layer thicknesses.[16]

In calculating the diffraction intensity, first we matched the Bragg peak positions and the overall profile with Co and Re layer thicknesses, the global interface roughness, and the background (which was almost constant for all the samples). Second, the layer-thickness fluctuation Δt (for simplicity, Δt was set equal for Co and Re layer thicknesses) were introduced in order to match the widths of the higher-order peaks. Then the interfacial mixing widths t_R and t_F were adjusted to decrease the higher-order peak intensities and to bring them in line with the measured values (here the subscripts R and F denote the interface configurations with Co deposited on a Re layer and with Re deposited on a Co layer, respectively. All multilayer samples studied here were deposited with a Re layer on top). Finally, the important parameters such as Co and Re individual layer thicknesses (t_{Co}, t_{Re}), the front and rear interfacial mixing widths (t_F, t_R), the rms interface roughness (σ_r), and the width of the layer-thickness distribution (Δt) were refined in a nonlinear least-squares fitting procedure which minimized the χ^2, defined in Eq. (1). The number of superlattice periods in the low-angle calculation was the actual number N of bilayers in the sample. The known electron densities and linear absorption coefficients[18] of bulk Co and Re were also used in the calculation.

Figure 2 shows the normalized x-ray-reflectivity data (open dots) for a set of equal-thickness Co/Re superlattice samples along with the fitted curves (solid line), with all corrections included, displayed on a semilogarithmic plot as a function of the scattering vector Q. The top Re layer of the samples gives a critical angle for total reflection of $\theta_c = 0.47°$ or $Q_c = 4\pi \sin(\theta_c)/\lambda = 0.067$ Å^{-1}. For samples with large periods Λ, the first Bragg peak

TABLE I. Parameters derived from the fitted rresults shown in Fig. 2 for two pairs of bilayer films. The t_0 is the oxide overlayer thickness, t_{Co} and t_{Re} are the Co and Re layer thicknesses, respectively, t_i is the interface thickness, and σ_r is the rms global interface roughness.

	glass/Co Å/Re Å	t_0 (Å)	t_{Co} (Å)	t_i (Å)	t_{Re} (Å)	σ_r (Å)
1	glass/Co120/Re60	~0	115.1±0.2	7.3±0.3	62.6±0.2	2.28±0.04
2	glass/Re160/Co35	30.7	5.6	~0	168.0	3.43
3	glass/Co70/Re35	~0	71.0	5.7	41.2	2.71
4	glass/Re75/Co35	18.0	27.8	~0	73.4	3.70

has a Q value (for example, for $\Lambda=220$ Å, $Q=0.085$ Å^{-1}) very close to Q_c, so it is difficult to resolve, as can be seen in Fig. 2 for samples A and B. As Λ decreases, the first Bragg peak shifts toward higher Q and becomes clearly resolved, as shown in Fig. 2 for smaller Λ. It is a well-known characteristic of superstructure peaks of equal-layer-thickness multilayers that the even-order reflection peaks have almost zero intensity. In Fig. 3, it is clearly observed that the intensities of the even-order reflection peaks are much smaller than those of the odd-order ones for samples with $\Lambda \geq 136$ Å , indicating that there is only a slight deviation from a square-wave modulation. For the samples with $\Lambda \leq 92$ Å, the deviation from the equal-thickness configuration becomes more evident.

The parameters derived from the fitted results are listed in Table II. The most interesting parameters obtained in the calculations are the front and real interfacial mixing widths, t_R and t_F, and the layer-thickness distribution width Δt. As can be seen in Table II, the values of t_F (~ 5 ML) are nearly 2 ML larger than that of the t_R (~ 3 ML) for all samples listed. This asymmetric interface configuration is in good agreement with the bilayer result. However, their values are about 2–3 ML larger than those obtained from the corresponding interface configurations in the bilayer samples. This result is not surprising, since it should be noted that, for multilayer samples, the front and rear intermixing widths derived from the low-angle reflectivity calculation are the averaged values over a larger number of interfaces across the film. There is now strong experimental evidence indicating that in some multilayer systems the layers become rougher as their distance from the substrate increases.[19,20] The larger t_R and t_F values found in our superlattice samples can then be attributed to the cumulatively increased layer roughness with increasing distance from the substrate. As far as the layer-thickness distribution width is concerned, Δt was observed to range from 1.2 to 4.1 Å in such a way that the ratio $2\Delta t/\Lambda$ remained constant around 3%. Finally, it should be noted that for the sample [Co25 Å/Re25 Å]$_{70}$, it was necessary to include in the calculation an additional top oxide overlayer with a thickness of 9 Å and 30% of the Re-electron density in order to fit the data adequately.

Samples with $\Lambda \leq 42$ Å prepared on glass substrates were found to be unstable, losing their mirror surface soon after deposition. Since the x-ray specular reflectivity is very sensitive to the film surface quality, the measured data for these samples were of insufficient quality to obtain a quantitative analysis of the low-angle x-ray

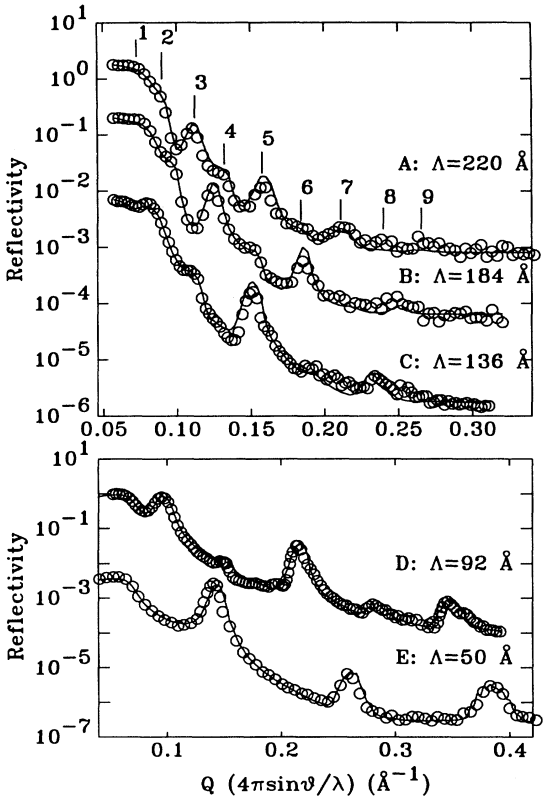

FIG. 2. X-ray-reflectivity data (circles), along with the fitted results (solid lines) for a set of equal-thickness Co/Re superlattice samples: A: $\Lambda=220$ Å, B: $\Lambda=184$ Å, C: $\Lambda=136$ Å, D: $\Lambda=92$ Å, and E: $\Lambda=50$ Å. For clarity, the curves have been displaced vertically and the angle peaks were indexed only for sample A.

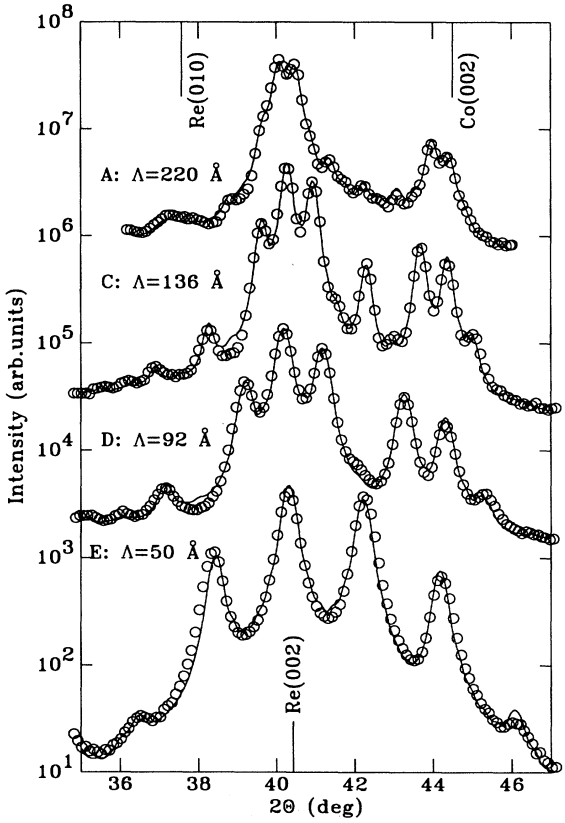

FIG. 3. High-angle x-ray-diffraction data (circles), along with the fitted results (solid line) for a series of equal-thickness Co/Re superlattice samples: A: $\Lambda=220$ Å, C: $\Lambda=136$ Å, D: $\Lambda=92$ Å, and E: $\Lambda=50$ Å. The positions corresponding to Co and Re reflections are indicated by the solid vertical lines. For clarity, the curves have been displaced vertically.

TABLE II. Derived parameters from fits to the low-angle reflectivity data shown in Fig. 3 for the Co/Re equal-thickness superlattices *A*, *B*, *C*, *D*, and *E*. The subscript *N* indicates the number of superlattice periods. Λ_s is the period, t_{Co} and t_{Re} are the Co and Re layer thicknesses, t_R and t_F are the rear (Co deposited on Re) and front (Re deposited on Co) interfacial mixing widths, respectively, Δt is the width of the layer-thickness distribution.

	$[\text{Co Å/Re Å}]_N$	Λ_s (Å)	t_R (Å)	t_{Co} (Å)	t_F (Å)	t_{Re} (Å)	Δt (Å)	σ_r (Å)
A	$[\text{Co110/Re110}]_{25}$	220.8	7.1±0.8	98.9±0.9	13.2±0.8	101.6±0.9	4.1±0.3	8.9±0.5
B	$[\text{Co92/Re92}]_{32}$	183.0	6.3	81.7	12.3	82.7	1.9	9.0
C	$[\text{Co68/Re68}]_{42}$	140.3	6.9	58.8	11.9	62.0	2.5	8.8
D	$[\text{Co46/Re46}]_{63}$	91.0	7.2	34.2	12.3	37.3	1.3	4.2
E	$[\text{Co25/Re25}]_{73}$	49.5	5.7	15.0	11.5	17.3	1.2	4.1

data, although the periods obtained from the observed Bragg peak positions were consistent with the targeted values.[21] In contrast, the samples with small periods prepared on oxidized silicon substrates for magnetoresistance studies are stable after preparation and their reflectivity data show sharp superlattice peaks for Λ down to 23 Å.[11] In any case, the results obtained from the bilayer and the equal-thickness multilayers characterize unambiguously the asymmetric interface configuration in these Co/Re superlattices. The average intermixing width in the superlattices was found to be ~2.5 ML at the interface with Co deposited on Re, and ~5 ML at the interface with Re deposited on Co. These results will be compared in Sec. V with those obtained from the analysis of high-angle x-ray-diffraction spectra in Sec. IV.

Finally, it should be noted that the present one-dimensional optical model does not permit us to distinguish interfaces which are truly diffuse from those which contain genuine roughness. However, low-angle rocking curves can give information on the real interface configurations.[22–25] Low-angle rocking curve measurements were performed on the Co/Re bilayer and multilayer films. Typical rocking curves show a strong specular peak (with a FWHM ~0.02°) accompanied by a diffuse scattering tail over an angular range of some ±0.4°. From the FWHM (~0.023°) of the specular peak of the rocking curve measured at the second Bragg peak for the Co/Re equal-thickness sample *A*, a lateral coherence length was estimated to be about 2000 Å. As shown in Refs. 22–24, the diffuse tails also contain information on the lateral correlation of the roughness, but further theoretical work is required for a complete interpretation.[25]

IV. HIGH-ANGLE X-RAY DIFFRACTION

Quantitative analysis of the high-angle x-ray-diffraction data has been performed using a trapezoidal model based on the kinematic theory of x-ray diffraction.[26] The model considers crystalline multilayer films having extended interfaces with linear composition profiles[26] in which the *d* spacings, atomic scattering factors, in-plane atomic densities, and Debye-Waller factors are all assumed to vary linearly across the two types of interfaces. This is equivalent to the linear variation of the refractive index across the interfaces in the low-angle reflectivity calculation and is a good approximation for systems which can form continuous solid solutions, such as the Co/Re studied here. Although probably oversimplified, this type of model adequately parametrizes the diffuse interface with a single variable. The model may include a small fraction of independent crystallites at other orientations.[26] The calculated intensity is then multiplied by an absorption correction,[27] the Lorentz-polarization factor,[27] and a scaling factor, and is also added to the background signal from the glass substrate. Finally, the instrumental broadening is introduced by convoluting the calculated intensity with a Lorentzian instrumental function.

The important adjusted parameters in the above model calculation are the average atomic spacings of Co and Re, $\bar{d}_{Co}$ and $\bar{d}_{Re}$, the corresponding atomic plane numbers n_{Co} and n_{Re}, the atomic layer numbers at the front and rear interfaces, n_F and n_R, and the coherence length of the multilayer crystallite along the growth direction L_c. The same fitting method, with σ^2 as defined in Eq. (2), was used as in the low-angle reflectivity data analysis. It should be reemphasized that the σ^2 defined in this manner is necessary in order to treat the data consistently over the whole range of intensities. In the preliminary analysis of the high-angle diffraction data using the trapezoidal model,[21] a standard form for χ^2 $[=\sum_{i=1}^{M}(R_i^m-R_i^c)^2/R_i^m]$ had been employed in the fitting procedure and resulted in the domination of strong high-order satellite peak on the value of χ^2. Within the trapezoidal model, the relative heights of the high-order satellites (which have lower intensities) to those of the low-order satellites (which have the strongest peak intensities) are sensitive to the number of interfacial atomic layers n_F and n_R. The fitting procedure with σ^2 given by Eq. (2) provides a more balanced weighting of low- and high-order satellites on the fitted results.

Discrete thickness fluctuations were simulated in the high-angle trapezoidal model in the same way as in the low-angle reflectivity calculation. It was found that a comparable amount of this discrete fluctuation (~1–2-ML width) cannot account for the observed high-angle peak width. A continuous fluctuation of lattice spacings within each layer of material has been considered as a possible origin for the observed width of the high-angle peak width,[4] but cannot be easily included within the trapezoidal model. Hence, for simplicity, the high-angle peak widths were determined by adjusting the length of

the multilayer crystallites, i.e., the number of atomic layers in the growth direction. Then the coherence length of the multilayer crystallite L_c is obtained from the number of bilayers needed to fit the width of multilayer peaks plus a fractional correction factor for additional broadening due to a nonintegral number of bilayers.[26] This coherence-length approach leads to a broadening of all peaks due to the finite size of the multilayers.

The high-angle x-ray-diffraction data (open dots) and refined calculation (solid line) for the Co/Re equal-thickness samples *A*, *C*, *D*, and *E* are shown in Fig. 3 on a semilogarithmic plot as a function of the scattering angle 2θ. Well-defined superlattice peaks have been observed in all samples, indicating coherent stacking of atomic planes across Co and Re layers. The intensities of the superlattice peaks are modulated by the structure factor of the bilayer so that the strongest superlattice peaks are found closest to the Bragg peaks of Re and Co hcp (002). For small Λ (50 and 41 Å), sharp superlattice peaks appear around the Bragg peaks corresponding to the Co and Re(002) average atomic spacing $d=\Lambda/N_p$, where N_p is the total number of atomic layers within a period. As can also be seen in Fig. 3, the angular distance between superlattice peaks decreases as the wavelength Λ increases. For the largest $\Lambda=220$ Å, the superlattice peaks were difficult to resolve with the low-resolution diffractometer used.

The structural parameters derived from the fitted results shown in Fig. 3 are listed in Table III. The sensitivity of the specific interface configuration (symmetric and asymmetric) and the number of atomic layers in the interface increases with decreasing wavelength Λ, but both were well determined for all samples by using σ^2 as defined in Eq. (2) to fit the data. As indicated in Table III, the average atomic spacings of (002) planes in all samples are apparently expanded by $\sim 0.6\%$ for Co and $\sim 0.3\%$ for Re compared with their bulk values (2.034 Å for Co and 2.229 Å for Re). However, an out-of-plane expansion of Co layers cannot be understood in terms of coherent strains at the superlattice interfaces, nor is it due to alloying of Co with Re, since interfacial mixing is limited in the large-Λ samples. The expansion of Co layers may arise as a result of structural disorder, which leads to a slight decrease in the packing density, as observed in the Co/Au multilayer system.[16] For the sample with $\Lambda=40$ Å, the expansion of the Co(002) planes becomes more important, but the Re(002) atomic spacings remains the same. It is proposed that this larger expansion of the Co layers in small-Λ samples arises from a small region in which Co alloys with Re, since the region near the interface becomes a larger fraction of the sample with small-Λ samples.

As can also be seen from Table III, the coherence length in the growth direction first increases with increasing Λ, passes through a maximum value for $\Lambda=136$ Å, then decreases. It should also be noted that the samples listed in Table III are essentially composed of only well-oriented hcp (002) multilayer crystallites, except for sample *A* with $\Lambda=220$ Å. The fitted results for sample *A* (shown in Fig. 3) includes a small fraction of Re crystallites with *d* spacing close to that of the (010) planes. In an earlier publication,[21] an [010]-oriented sample with $\Lambda=14$ Å was found to grow coherently for about 14 bilayers and consisted only of interface layers arising from the intermixing of the rough interface regions within the sample.

Finally, rocking curves were measured at the two strongest superlattice peaks around the Bragg peaks of Re and Co(002) for large-Λ samples. For small-Λ samples (50 and 42 Å), only one rocking curve was measured at the strongest superlattice peak position. The FWHM's of the rocking curves are almost the same (about 6.2°) for all samples with large Λ, indicating that the texture is nearly identical within the Co and Re layers in these large-Λ samples. For $\Lambda \leq 50$ Å, the FWHM was found to be larger, about 10.0°. The broadening of the rocking curve is ascribable both to the coherence length of the diffracted x rays in the film plane and the orientational distribution of the crystallites (mosaic spread). In order to probe the coherence length within the film plane, a symmetric transmission scan with the scattering vector Q in the film plane was performed for the largest Λ (220 Å) sample. A relative strong peak corresponding to the (010) reflection accompanied by a very weak (101) reflection peak of hcp Re was observed in the transmission diffraction profile. No reflection peak from Co was detected in this geometry, due to its relatively small atomic scattering factor. From the FWHM of the (010) peak of hcp Re, the in-plane coherence length within the Re layer was calculated using the Scherrer equation to be about 100 Å.[27] As a rough approximation, the rocking curve can be reproduced by the convolution of two Lorentzian curves representing the broadening due to the in-plane crystallographic coherence length and the distri-

TABLE III. Derived parameters from fits to the high-angle diffraction data for the Co/Re equal-thickness superlattices *A*, *B*, *C*, *D*, *E* and *F*. $\bar{d}_{Co}$ and $\bar{d}_{Re}$ are the average atomic interplanar distances of Co and Re(002), n_{Co} and n_{Re} the corresponding atomic plane numbers, n_R and n_F the atomic layer numbers at the rear and front interfaces, and L_c the coherence length of the multilayer crystallite along the growth direction.

	$[Co\ Å/Re\ Å]_N$	Λ_h (Å)	$\bar{d}_{Co}$ (Å)	$\bar{d}_{Re}$ (Å)	n_R	n_{Co}	n_F	n_{Re}	L_c (Å)
A	$[Co110/Re110]_{25}$	218.2	2.046±0.004	2.241±0.004	3	49	6	44	324
B	$[Co92/Re92]_{32}$	181.8	2.047	2.240	2	41	5	37	347
C	$[Co68/Re68]_{42}$	138.7	2.045	2.233	2	30	6	27	392
D	$[Co46/Re46]_{63}$	91.9	2.046	2.239	2	19	5	17	234
E	$[Co25/Re25]_{73}$	49.1	2.043	2.234	3	8	4	8	244
F	$[Co19/Re23]_{85}$	40.8	2.063	2.236	2	7	3	7	251

bution function for the mosaic spread, respectively. The FWHM of the former at the strongest superlattice peak around Re(002) is calculated from the observed in-plane coherence length to be about 1.0°. By deconvoluting this width from that of the observed rocking curve, the FWHM of the orientational function is estimated to be 5.2°. Therefore, the broadening of the rocking curves is dominated in our samples by the mosaic spread.

V. COMPARISON OF LOW- AND HIGH-ANGLE DIFFRACTION RESULTS

As is also evident from Table III, the values of n_R and n_F from the high-angle analysis indicate asymmetric interface configurations, consistent with the low-angle reflectivity results. It is interesting to compare $n_R(\bar{d}_{Co}+\bar{d}_{Re})/2$ (rear interface thickness), $n_{Co}\bar{d}_{Co}$ (Co layer thickness), $n_F(\bar{d}_{Co}+\bar{d}_{Re})/2$ (front interface thickness), and $n_{Re}\bar{d}_{Re}$ (Re layer thickness) (see Table III) with the corresponding values of t_R, t_{Co}, t_F, and t_{Re} (see Table II) obtained from the fits to the low-angle reflectivity data. The former four values are calculated from Table III and are listed in Table IV. As can easily be seen from Tables II and IV, the agreement is quite good. The interfacial mixing widths were found to be slightly larger in the low-angle results than in the high-angle ones, in particular for rear interfaces. When comparing the high- and low-angle calculations, it should be kept in mind that, in the high-angle trapezoidal model, the peak widths were determined by the multilayer crystallite length. As mentioned above, a better model of high-angle diffraction would include both discrete and continuous layer-thickness fluctuations to account for the observed peak widths, but this requires a closed form in the trapezoidal model calculation.[4] Since the incorporation of discrete and continuous layer-thickness fluctuations in the trapezoidal model calculation would affect the relative intensities of the main peaks and the high-order satellites, the values of n_R and n_F obtained in the actual fits to high-angle data may not be very accurate. On the other hand, since low-angle reflectivity data are much more sensitive to discrete rather than continuous layer-thickness disorder,[4] our low-angle fitted results should be quite accurate since they are less affected by the absence of continuous layer-thickness fluctuations in the optical model calculation.

Low-angle reflectivity does not depend on the atomic structure of the layers and, in consequence, the coherence lengths [in the film plane (typically over 1000 Å) as well as in the growth direction] were usually found to be much larger than those in high-angle diffraction data.[16] Furthermore, the low incident angle of the reflectivity experiment results in the larger lateral sample area illuminated by the x-ray beam as well as a limited penetration depth (~3000 Å). Hence, low-angle scattering averages over a larger lateral region of the sample near the free surface than is the case for the high-angle diffraction, which averages over the entire sample thickness with a sample area determined approximately by the x-ray beam size. For a layer roughness which increases with distance from the substrate, larger interfacial mixing widths are expected in low-angle reflectivity than in high-angle diffraction, as found for our Co/Re multilayer films. As can be seen in Tables II and IV, the intermixing widths found from the fits to the reflectivity data are larger than those found in the high-angle intensity calculations, in particular for the small-Λ samples.

VI. SUMMARY AND CONCLUSIONS

The structural properties of a series of sputtered Co/Re equal-thickness superlattices and several bilayer films have been investigated by low- and high-angle x-ray diffraction. Low-angle reflectivity data have been analyzed using an optical model which includes both the interfacial mixing and the discrete layer-thickness fluctuations. The fits to the reflectivity data of the bilayer samples indicate that the interfacial mixing width is confined to 2–3 ML for Re deposited on Co, and < 1 ML for Co deposited on Re. The fitted results from superlattice samples are consistent with this asymmetric interface configuration. Somewhat larger average interfacial widths (~3–5 ML) were found in Co/Re superlattices, and are attributed to the cumulatively increasing layer roughness with increasing distance of the layers from the substrate.

The high-angle x-ray-diffraction data demonstrate that these Co/Re equal-thickness samples have coherent and highly textured structures with hcp [002] orientation normal to the film plane. The fitted results of the high-angle x-ray data using a trapezoidal model are in good agreement with the ones obtained from the reflectivity data analysis. Comparing the results obtained from the low- and high-angle experiments, we can characterize unambiguously the asymmetric interface configuration in these Co/Re superlattices with an average intermixing width ~2.5 ML at Co on Re interfaces, and ~5 ML at Re on Co interfaces. A systematic expansion of the Co(002) layer is observed in all the samples studied here, and is inter-

TABLE IV. The calculated values of $n_R(\bar{d}_{Co}+\bar{d}_{Re})/2$ (rear interface thickness), $n_{Co}\bar{d}_{Co}$ (Co layer thickness), $n_F(\bar{d}_{Co}+\bar{d}_{Re})/2$ (front interface thickness), and $n_{Re}\bar{d}_{Re}$ (Re layer thickness) from Table III.

	$[Co Å/Re Å]_N$	$n_R(\bar{d}_{Co}+\bar{d}_{Re})/2$	$n_{Co}\bar{d}_{Co}$	$n_F(\bar{d}_{Co}+\bar{d}_{Re})/2$	$n_{Re}\bar{d}_{Re}$
A	$[Co110/Re110]_{25}$	6.4 (Å)	100.3 (Å)	12.9 (Å)	98.6 (Å)
B	$[Co92/Re92]_{32}$	4.3	83.9	10.7	82.9
C	$[Co6/Re68]_{42}$	4.3	61.4	12.8	60.3
D	$[Co46/Re46]_{63}$	4.3	38.9	10.7	38.1
E	$[Co25/Re25]_{73}$	4.3	16.3	10.6	17.9

preted as the result of an imperfectly stacked structure leading to a reduced atomic density.

The asymmetry between Co on Re and Re on Co interfaces is not entirely surprising. On the one hand, it may arise from the thermodynamics of the growing interface, or, on the other hand, it can result from the kinetics of the sputtering process. In this regard, we note that a similar asymmetry has been detected in sputter-deposited Mo/Si (Refs. 28 and 29) and tungsten carbide–cobalt (WC/Co) (Ref. 30) multilayers. In all these systems, the interfacial mixing is larger when the heavier atom is deposited on the lighter, suggesting that the kinematics of the impact process may be the important element. Systematic studies of layers produced under different sputtering conditions, or even by other techniques, are required in order to shed further light on this interesting phenomenon.

ACKNOWLEDGMENTS

We would like to thank H. E. Fischer for his help with the x-ray-reflectivity data analysis, and Y. Shi and Y. Xu for their assistance during the x-ray-diffraction measurements. Y.H. wishes to thank T. Moreno for valuable discussions. We acknowledge financial support for this research from NSERC, Canada and FCAR, Quebec.

---

*Present address: Institut National de la Recherche Scientifique—Énergie et Matériaux, 1650 montée Sainte-Julie, Case Postale 1020, Varennes, Québec, Canada J3X 1S2.

[1]M. N. Baibich, J. M. Broto, A. Fert, F. Nguyen van Dau, F. Petroff, P. E. Etienne, G. Creuzet, A. Friederich, and J. Chazelas, Phys. Rev. Lett. **61**, 2472 (1988); S. S. P. Parkin, R. Bhadra, and K. P. Roche, *ibid.* **66**, 2152 (1991).

[2]F. J. A. den Broeder, W. Hoving, and P. J. H. Bloemen, J. Magn. Magn. Mater. **93**, 562 (1991).

[3]For recent review, see, for example, D. B. McWhan, in *Physics, Fabrication and Applications of Multilayered Structures,* edited by P. Dhez and C. Weisbuch (Plenum, New York, 1988), p. 67.

[4]E. E. Fullerton, I. K. Schuller, H. Vanderstraeten, and Y. Bruynseraede, Phys. Rev. B **45**, 9292 (1992).

[5]M. F. Toney and S. Brennan, J. Appl. Phys. **66**, 1861 (1989).

[6]Y. Huai and R. W. Cochrane, J. Appl. Phys. **72**, 2523 (1992).

[7]A. R. Miedema, Philips Tech. Rev. **36**, 217 (1976).

[8]F. A. Shunk, *Constitution of Binary Alloys,* 2nd Suppl. (McGraw-Hill, New York, 1969), p. 495.

[9]Y. Huai and R. W. Cochrane (unpublished).

[10]Y. Huai, Ph.D thesis, Université de Montréal, 1993.

[11]Y. Huai, R. W. Cochrane, and M. Sutton, J. Appl. Phys. **73**, 5530 (1993); Y. Huai, R. W. Cochrane, Y. Shi, H. E. Fischer, and M. Sutton (unpublished).

[12]M. Born and E. Wolf, *Principles of Optics* (Pergamon, Oxford, 1964), p. 57.

[13]B. K. Agarwal, *X-Ray Spectroscopy* (Springer, Berlin, 1979), p. 134.

[14]D. G. Stearns, J. Appl. Phys. **65**, 491 (1989); **71**, 4286 (1992).

[15]R. W. James, *The Optical Principles of Diffraction of X-Rays* (Cornell University Press, New York, 1965).

[16]F. J. Lamelas, H. David He, and Roy Clarke, Phys. Rev. B **43**, 12 296 (1991).

[17]J.-P. Locquet, D. Neerinck, L. Stockman, Y. Bruynseraede, and I. K. Schuller, Phys. Rev. B **39**, 13 338 (1989).

[18]B. E. Warren, *X-Ray Diffraction* (Addison-Wesley, Reading, MA, 1968).

[19]M. B. Stearns, C. H. Lee, C. H. Chang, and A. K. Petford-Long, in *Metallic Multilayers and Epitaxy,* edited by M. Hong, S. Wolf, and D. C. Gubser (The Metallurgical Society of AIME, Denver, 1988).

[20]E. E. Fullerton, D. M. Kelly, J. Guimpel, I. K. Schuller, and Y. Bruynseraede, Phys. Rev. Lett. **68**, 859 (1992).

[21]Y. Huai, R. W. Cochrane, Y. Shi, H. E. Fischer, and M. Sutton, in *Structure & Properties of Interfaces in Materials,* edited by W. A. T. Clarke, C. L. Briant, and U. Dahmen, MRS Symposia Proceedings No. 238 (Materials Research Society, Pittsburgh, 1992), p. 671.

[22]S. K. Sinha, Physica B **173**, 25 (1991).

[23]D. E. Savage, J. Kleiner, N. Schimke, Y. H. Phang, T. Jankowski, J. Jacobs, R. Kariotis, and M. G. Lagally, J. Appl. Phys. **69**, 1411 (1991).

[24]R. Chiarello, V. Panella, J. Krim, and C. Thompson, Phys. Rev. Lett. **67**, 3408 (1991).

[25]J. B. Kortright, J. Appl. Phys. **70**, 3620 (1991).

[26]M. B. Stearns, C. H. Lee, and T. L. Groy, Phys. Rev. B **40**, 8256 (1989); M. B. Stearns, *ibid.* **38**, 521 (1989).

[27]A. Guinier, *X-Ray Diffraction in Crystals, Imperfect Crystals, and Amorphous Materials* (Freeman, San Francisco, 1963).

[28]C. Montcalm, B. T. Sullivan, H. Pépin, J. J. Dubowski, and M. Sutton (unpublished).

[29]M. B. Stearns, C. H. Chang, and D. G. Stearns, J. Appl. Phys. **71**, 187 (1992); J. Slaughter, P. A. Kearney, D. W. Schulze, C. M. Falco, C. R. Hills, E. B. Soloman, and R. N. Watts, Proc. SPIE **1343**, 73 (1990).

[30]T. D. Moustakas, J. Y. Koo, A. Ozekcin, and J. Scanlon, J. Appl. Phys. **65**, 4256 (1989).